JFM RAPIDS
journals.cambridge.org/rapids

Non-specular reflection of walking droplets

Giuseppe Pucci[1,2], **Pedro J. Sáenz**[1], **Luiz M. Faria**[1]
and John W. M. Bush[1,†]

[1]Department of Mathematics, Massachusetts Institute of Technology, Cambridge, MA 02139, USA

[2]The Hatter Department of Marine Technologies, University of Haifa, Haifa, 3498838, Israel

Since their discovery by Yves Couder and Emmanuel Fort, droplets walking on a vibrating liquid bath have attracted considerable attention because they unexpectedly exhibit certain features reminiscent of quantum particles. While the behaviour of walking droplets in unbounded geometries has to a large extent been rationalized theoretically, no such rationale exists for their behaviour in the presence of boundaries, as arises in a number of key quantum analogue systems. We here present the results of a combined experimental and theoretical study of the interaction of walking droplets with a submerged planar barrier. Droplets exhibit non-specular reflection, with a small range of reflection angles that is only weakly dependent on the system parameters, including the angle of incidence. The observed behaviour is captured by simulations based on a theoretical model that treats the boundaries as regions of reduced wave speed, and rationalized in terms of momentum considerations.

Key words: capillary waves, drops, Faraday waves

1. Introduction

Ten years ago, Yves Couder and Emmanuel Fort discovered that a millimetric drop placed on a vibrating fluid bath may interact with its own wave field in such a way as to walk steadily across the surface (Couder *et al.* 2005; Protière, Boudaoud & Couder 2006). These walking droplets, henceforth 'walkers', are composed of both droplet and extended wave, and exhibit several features previously thought to be exclusive to the microscopic, quantum realm (see reviews by Bush 2015*a*,*b*). Integrated experimental and theoretical work has rationalized the manner in which chaotic pilot-wave dynamics may give rise to quantum-like statistical behaviour in unbounded geometries, for example in orbital dynamics (Fort *et al.* 2010; Harris & Bush 2014; Labousse *et al.* 2014, 2016; Oza *et al.* 2014; Perrard *et al.* 2014*a*,*b*). The interaction of walkers with boundaries, as arises in a number of key quantum

† Email address for correspondence: bush@math.mit.edu

analogue systems (Couder & Fort 2006; Eddi *et al.* 2009; Harris *et al.* 2013; Gilet 2014, 2016), remains relatively poorly understood.

In their experimental investigation of walkers tunnelling across submerged barriers, Eddi *et al.* (2009) noted the predominance of a single reflection angle of approximately 60° (measured with respect to the normal) when the walker bounced off the walls of a square cavity. Indeed, this reflection behaviour was exploited in the development of their experimental arrangement. Couder & Fort (2006) showed that walkers exhibit single-particle diffraction and interference when they pass through single- or double-slit geometries. Recently, Andersen *et al.* (2015) and Batelaan *et al.* (2016) revisited these experiments and found results at odds with those of Couder & Fort (2006). Harris (2015) examined the diffraction of walkers through a slit, and found the behaviour to be dominated by wall effects. Specifically, there was a preferred diffraction angle of approximately 60°, comparable to the angle of reflection of a walker from a planar boundary.

A prerequisite for the theoretical rationale of the behaviour in the diffraction and interference experiments would thus seem to be the understanding of the interaction of walkers with relatively simple boundary geometries. We here examine experimentally and theoretically the interaction of walking droplets with a planar submerged barrier. Specifically, in §2, we characterize the reflection laws of walking droplets experimentally, then in §3 capture the observed behaviour with simulations based on a recently developed theoretical model (Faria 2016). The rationale for the non-specular reflection is provided in §4 on the basis of existing reduced theoretical models of the walker dynamics (Bush, Oza & Molácek 2014; Labousse & Perrard 2014).

2. Experiments

The fluid bath is composed of silicone oil with viscosity $\nu = 20.9$ cSt, density $\rho = 950$ kg m^{-3} and surface tension $\sigma = 20.6$ mN m^{-1}. A schematic of the set-up is presented in figure 1. The bath is circular with diameter 15.8 cm, depth $h_0 = 6.09 \pm 0.03$ mm and is surrounded by a shallow border of width 12.7 mm and depth 1.3 mm that acts as a wave damper, thus minimizing the interaction of the walker with the outer boundary. A stainless steel barrier (visible on the right of figure 1*b*) is bolted to an aluminium base plate and serves as the reflecting planar boundary. On the barrier, the fluid depth is reduced to $h_1 = 0.42 \pm 0.03$ mm, which is too shallow to support a walking drop. This depth h_1 was chosen to correspond most closely to that used by Harris (2015) for the single-slit diffraction experiments. The barrier is 30 mm wide so that the droplets cannot tunnel across it (Eddi *et al.* 2009) and waves do not propagate beyond it.

The bath is driven at the frequency $f_0 = 80$ Hz by an electromagnetic shaker with acceleration $\Gamma(t) = \gamma \cos(\omega t)$, where $\omega = 2\pi f_0$. The drive shaft is guided by a linear air bearing that ensures a spatially uniform vertical vibration to within 0.1%. The forcing is controlled by a closed-loop feedback that ensures a constant acceleration amplitude to within ± 0.002 g (Harris & Bush 2015), and monitored by two accelerometers placed symmetrically with respect to the centre of the bath. For $\gamma \geqslant \gamma_F \simeq 4.2$ g, the Faraday instability arises on the bath, resulting in standing gravity–capillary waves of wavelength $\lambda_F = 4.75$ mm and frequency $f_0/2$ (Faraday 1831). We examine droplets walking below this threshold, so that the dimensionless acceleration, henceforth referred to as the 'forcing amplitude', $\gamma/\gamma_F < 1$. The experimental uncertainty in γ/γ_F is less than 0.2% and due primarily to the small variation of the Faraday
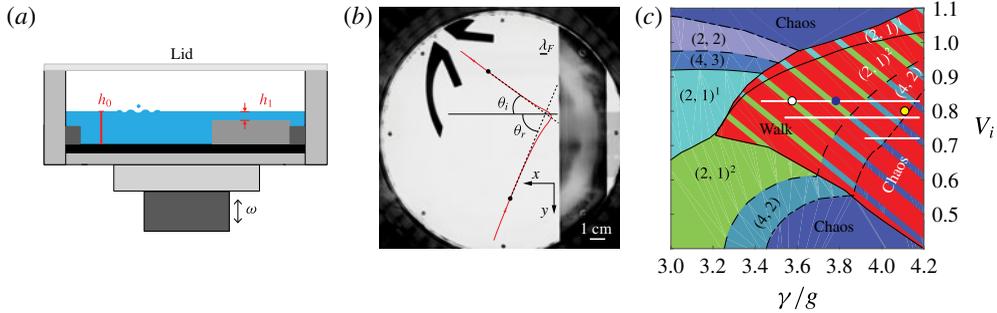
FIGURE 1. (a) Experimental set-up (not to scale). In the vicinity of the reflecting barrier, the fluid depth is reduced from $h_0 = 6.09 \pm 0.03$ mm to $h_1 = 0.42 \pm 0.03$ mm. (b) Typical trajectory (in red) of a walking droplet reflecting off the planar boundary. The droplet is launched from a submerged V-shaped launcher (in black) towards the reflecting barrier (in grey). The local angle of incidence θ_i and reflection θ_r at the two black points are indicated. (c) Parameter regimes of bouncing and walking drops indicating the dependence of the bouncing state (m, n) on the dimensionless acceleration γ/g and the vibration number $V_i = \omega/\sqrt{\sigma/\rho R^3}$, where R is the drop radius (Molacek & Bush 2013b). In the $(m, n)^k$ mode, the drop bounces n times in m driving periods. $(2, 1)^1$ and $(2, 1)^2$ denote resonant walkers with a different mean mechanical energy. The white segments indicate the parameter regimes explored in our study. White and blue circles correspond to the droplets used in figure 3(c), while the yellow circle corresponds to that used for the visualization of the wave field in figure 6.

threshold during the course of the experiments, as arises due to the dependence of the fluid viscosity on temperature. The forcing amplitude uniquely defines the memory parameter $M_e = T_d/[T_F(1 - \gamma/\gamma_F)]$, where T_d is the wave decay time in the absence of vibration and $T_F = 2/f_0$ is the period of the Faraday waves (Eddi *et al.* 2011; Molacek & Bush 2013b). M_e gives an estimation of the number of past bounces that contribute to the build-up of the instantaneous guiding wave field. Throughout this paper we will refer alternatively to the forcing amplitude and the memory.

Droplets of the same silicone oil as the bath are generated via the droplet-on-demand generator developed by Harris, Liu & Bush (2015), which reduces uncertainty in the drop diameter D to ± 0.01 mm. Droplets are released onto the vibrating bath along a slide painted with a thin layer of silicone oil. The parameter regime of the drops used in this work is highlighted in figure 1(c). We explored the behaviour of walking drops of three different sizes in the resonant $(2, 1)^2$ mode, in the $(4, 2)$ mode and in the chaotic regime arising at high memory for relatively small drops (Molacek & Bush 2013b; Wind-Willassen *et al.* 2013). The container is sealed with a transparent acrylic lid to isolate the droplet from ambient air currents. Walkers were directed towards the barrier with a V-shaped launcher (see figures 1(b) and 2), above which the fluid depth was reduced to 0.6 mm. At the exit of the launcher, droplets follow a straight path until they start interacting with the reflecting barrier. After the reflection event, they usually follow the outer wall until returning to the launcher, which allowed for repeated measurements in the same experimental conditions. The initial angle of incidence was controlled by shifting the position of the launcher.

The walker motion was recorded with a CCD camera at 10 frames per second and tracked with an in-house particle-tracking algorithm. Angles were measured locally along the trajectories by considering the tangent line at the point of measurement and
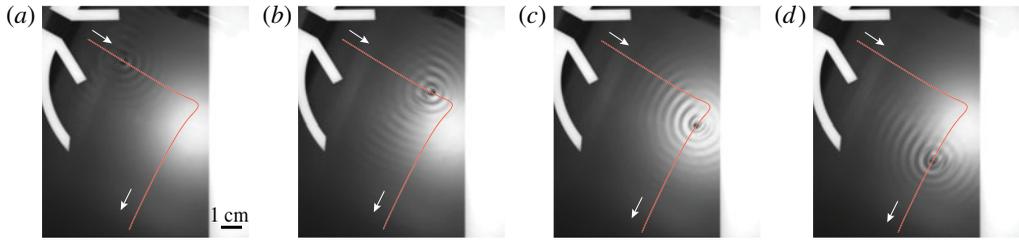
G. Pucci, P. J. Sáenz, L. M. Faria and J. W. M. Bush

FIGURE 2. Four snapshots of a walking droplet with its wave field as it is reflected from a submerged barrier (in white). (*a*) $t = 1.2$ s, (*b*) $t = 4.4$ s, (*c*) $t = 7.1$ s, (*d*) $t = 9.4$ s.
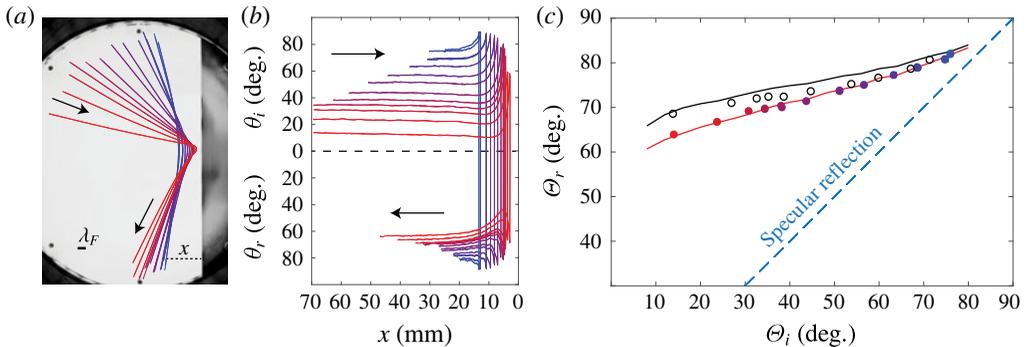

FIGURE 3. Non-specular reflection of a walking droplet of diameter $D = 0.78$ mm. At $\gamma/\gamma_F = 0.900$, its free speed is $v_0 = 11.45 \pm 0.10$ mm s^{-1}. (*a*) Trajectory colour varies from blue to red as the initial incidence angle Θ_i decreases. The launcher is removed from the image for the sake of clarity. (*b*) Local measurements of the angle of incidence θ_i and reflection θ_r as a function of the distance x from the barrier. (*c*) The final reflection angle Θ_r as a function of the initial incidence angle Θ_i for $\gamma/\gamma_F = 0.900$ (full circles) and $\gamma/\gamma_F = 0.850$ (open circles). These walkers are identified respectively by the blue and white circles in figure 1(*c*). Experiments are compared to the results from the theoretical model (red and black solid lines, respectively) and the specular reflection law $\Theta_r = \Theta_i$ (dashed line).

the first four neighbours. The angle between this line and the normal to the barrier was defined to be the local angle of incidence θ_i or reflection θ_r (figure 1*b*) along, respectively, the incoming and outgoing portions of the trajectory. In the far field, θ_i and θ_r asymptote to the initial angle of incidence Θ_i and the final angle of reflection Θ_r, respectively. Θ_i is defined as the average over the first 10 values of θ_i at the exit of the launcher, and Θ_r similarly by the average over the last 10 values of θ_r.

First, we characterize the dependence of the final reflection angle Θ_r on the initial incident angle Θ_i at relatively low memory. We consider a droplet of diameter $D = 0.78$ mm at two accelerations, $\gamma/\gamma_F = 0.850$ and $\gamma/\gamma_F = 0.900$, where it is a resonant $(2, 1)^2$ walker with respective speeds $v_0 = 10.6 \pm 0.1$ mm s^{-1} and $v_0 = 11.45 \pm 0.10$ mm s^{-1}. For each Θ_i, we repositioned the launcher so that the walker impinges close to the centre of the barrier. We then resealed the container, and recorded at least two trajectories. These trajectories were indistinguishable within the errors of our experimental set-up. At these low memories, the trajectory is uniquely determined by the initial incident angle Θ_i.
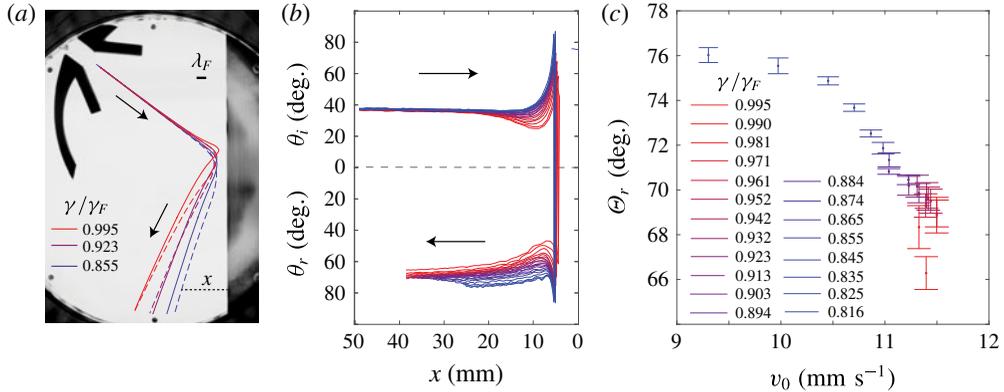
FIGURE 4. Dependence on memory, γ/γ_F, of the reflection of a walker of diameter $D = 0.78$ mm for a fixed initial angle of incidence $\Theta_i = 37.3 \pm 0.5°$. The path through parameter space is indicated by the uppermost white line segment in figure 1(c). Colour changes from blue to red as γ/γ_F increases. (a) Three experimental trajectories (solid lines) compared to computed trajectories (dashed lines). (b) Local measurement of the incidence angle θ_i and the reflection angle θ_r as a function of the distance from the barrier x. (c) Final reflection angle Θ_r as a function of the drop free speed v_0. The error on the latter is $\Delta v_0 = 0.05$ mm s^{-1}.

In figure 3(a) we report one trajectory per Θ_i. The reflection is clearly non-specular: $\Theta_r \neq \Theta_i$. Moreover, we observe that a wide range of Θ_i converges to a narrow band of Θ_r in the vicinity of 70°. This convergence is evident in figure 3(b), where the local angle is reported for each trajectory as a function of the normal distance from the barrier x. At the exit of the launcher, the walker proceeds in a rectilinear fashion. As it approaches the barrier, the local angle of incidence θ_i generally increases. After the walker reverses direction, θ_r changes continuously before approaching its final value Θ_r in the far field, where the walker proceeds again in a rectilinear fashion. The reflection process occurs over a time interval of several seconds, during the course of which the walker interacts with the planar barrier through its wave field. We note that along both the incident and reflected trajectories, the walker curves towards the barrier, except during its relatively abrupt reversal of direction, as arises at a distance from the barrier that depends on Θ_i but is in the range 0.6–$2.8\lambda_F$. The final reflection angle Θ_r is plotted as a function of the initial incidence angle Θ_i in figure 3(c), where the deviation from specular reflection is again apparent. For $\gamma/\gamma_F = 0.900$, the wide range of initial angles of incidence $\Theta_i \in [14°, 76°]$ results in a relatively narrow band of final reflection angles $\Theta_r \in [64°, 82°]$. For $\gamma/\gamma_F = 0.850$, the wide range of initial angles of incidence $\Theta_i \in [14°, 71°]$ results in an even narrower band of final reflection angles $\Theta_r \in [69°, 81°]$.

We also investigated the influence of memory on the reflection of droplets of diameter $D = 0.78$ and 0.75 mm with a fixed Θ_i. In figure 4(a) we present trajectories of the drop of diameter $D = 0.78$ mm. Both incident and reflected trajectories vary with memory. In the approach phase, the low-memory walker senses the barrier at a distance $x \approx 10$ mm from the barrier. The high-memory walker senses the barrier earlier owing to its relatively extended wave field. These features are highlighted in figure 4(b), where the local angle is plotted for each trajectory as a function of the distance from the barrier x. We note that the local minimum in the angle
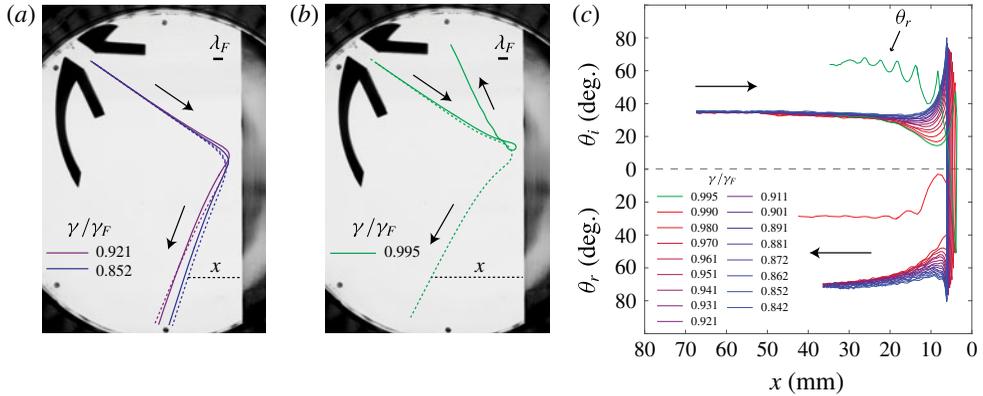
FIGURE 5. Dependence on memory γ/γ_F of the reflection of a walker of diameter $D = 0.75$ mm for a fixed initial angle of incidence $\Theta_i = 34.9 \pm 0.6°$ (indicated by the middle white line segment in figure 1c). Comparison of experimental (solid line) and theoretical (dashed line) trajectories at (a) two low memories and (b) one very high memory, where an anomalous trajectory is observed in the experiments but not in the model. (c) Local measurement of the angle of incidence θ_i and the reflected angle θ_r as a function of the distance x from the barrier at different memories. The anomalous trajectory presented in (b) is highlighted in green.

of incidence θ_i in the vicinity of the barrier decreases as the memory increases. In figure 4(c), the dependence of Θ_r on the drop free speed v is reported for the different memories examined. At the highest memories considered, we were at the limit of our experimental configuration: at the edge of the domain, the walker trajectories were still slightly curved. We note here that Θ_r remains constant for γ/γ_F from 0.894 to 0.981. In this memory range, the speed is nearly constant, indicating that Θ_r is more sensitive to the drop free speed than to memory. The overall spread of the reflected trajectories in this set of experiments is in the range $\Theta_r \in [66°, 76°]$, with higher speeds corresponding to lower reflection angles. We conclude that Θ_r decreases monotonically with the drop's free speed.

In figure 5(a,b), we present trajectories in the same experimental conditions for a smaller droplet, with diameter $D = 0.75$ mm, whose speed at $\gamma/\gamma_F = 0.901$ is $v_0 = 9.15 \pm 0.10$ mm s^{-1}. The behaviour is very similar to that arising for $D = 0.78$ mm except at high γ/γ_F, where the reflection angle may decrease dramatically (at $\gamma/\gamma_F = 0.990$) or even take on negative values (at $\gamma/\gamma_F = 0.995$). In the latter case, the droplet executes a loop whose diameter is approximately one Faraday wavelength, before exiting the loop and wobbling towards rectilinear motion (figure 5b). The loop is presumably due to a transient self-confinement of the walker in its own wave field, as has been discussed elsewhere (Labousse 2014; Oza *et al.* 2014; Bush 2015b). In figure 5(c), oscillations at high memory are clearly evident. While this slower walker asymptotes to Θ_r more slowly than its faster counterpart, the band of final reflection angles is clearly narrower. However, it is difficult here to assess reliably the dependence of Θ_r on memory and drop speed as trajectories are still curved at the limit of the experimental set-up. Equivalent experiments with an even smaller drop ($D = 0.71$ mm, lowermost white horizontal line in figure 1(c), for which $v_0 = 6.8 \pm 0.1$ mm s^{-1} at $\gamma/\gamma_F = 0.900$) show that reflection angles are
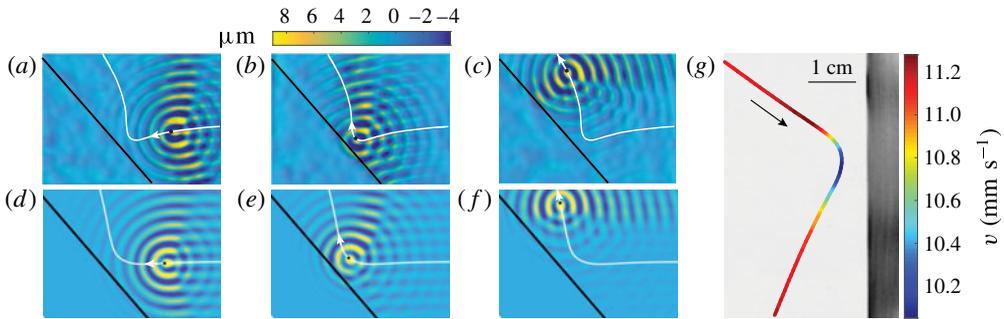
FIGURE 6. Experimental (*a*–*c*) and theoretical (*d*–*f*) wave fields as the walker reflects from a planar barrier. Drop diameter $D = 0.76$ mm and free speed $v_0 = 11.2$ mm s^{-1}, height above the barrier $h_1 = 0.3$ mm and in the deep region $h_0 = 10$ mm, forcing amplitude $\gamma/\gamma_F = 0.979$ (yellow circle in figure 1*c*). (*g*) Speed variation in the vicinity of the barrier of a drop with $D = 0.78$ mm at $\gamma/\gamma_F = 0.903$ with $h_1 = 0.42 \pm 0.03$ mm (blue circle in figure 1*c*). Surface Schlieren images (*a*–*c*) are taken with the bath at its maximal vertical displacement (courtesy of P.-T. Brun and A. Damiano).

confined to an even narrower band and reversed reflection occurs at a lower memory, specifically for $\gamma/\gamma_F = 0.981$. Above this forcing amplitude, for a given Θ_i, different reversed reflection angles can be obtained, suggesting chaotic reflection dynamics. We note that this apparently chaotic dynamics may result from the chaotic vertical dynamics arising for such a drop at high memory: the rightmost edge of the relevant lower white segment in figure 1(*c*) lies within a chaotic bouncing regime.

We also examined the reflection of the larger droplet ($D = 0.78$ mm) at $\gamma/\gamma_F = 0.950$ and $\gamma/\gamma_F = 0.990$. At such high memories, however, it was again impossible to measure the final angle of reflection Θ_r because the drop trajectories were still curved at the limits of the experimental domain. For $\gamma/\gamma_F = 0.990$ and $\Theta_i \leqslant 30°$, Θ_r decreases dramatically, and at small Θ_i the drop loops around its own wave field in the vicinity of the barrier and executes reversed reflection. Finally, we investigated the reflection behaviour of a slow drop with diameter $D = 0.71$ mm at $\gamma/\gamma_F = 0.900$ and $\gamma/\gamma_F = 0.850$. Here again, the trajectories are still slightly curved at the limit of the experimental set-up, so it is not possible to measure Θ_r. However, we could ascertain that the non-specularity is enhanced: larger values of Θ_r are obtained and lie in a relatively narrow range.

We also investigated the influence of the fluid depth h_1 above the barrier by exploring the behaviour at $h_1 = 0.04 \pm 0.03$ mm and $h_1 = 0.81 \pm 0.03$ mm. Reflection maintains the feature of non-specularity with $\Theta_r \approx 70°$. A slight decrease of Θ_r with the drop free speed was apparent, as was the case when $h_1 = 0.42$ mm.

3. Theoretical modelling

Recently, a reduced model that captures many features observed in experiments has been developed by Faria (2016). Its key feature is that it incorporates the dependence of wave speed on fluid depth in a simple way, and so enables the treatment of walker–boundary interactions. This model builds upon that of Milewski *et al.* (2015) by making the simplifying assumption that the waves are monochromatic; therefore, only waves with Faraday frequency need be considered.

For completeness, we recall the governing equations of Milewski *et al.* (2015) which, when extended to a bath of finite depth, are given by:

$$\Delta\phi = 0, \quad \text{for } -h(\boldsymbol{x}) \leqslant z \leqslant 0, \tag{3.1}$$

$$\nabla\phi \cdot \boldsymbol{n} = 0, \quad \text{for } z = -h(\boldsymbol{x}), \tag{3.2}$$

$$\phi_t = -g(t)\eta + 2\nu^*\nabla_\perp^2\phi + \frac{\sigma}{\rho}\nabla_\perp^2\eta - \frac{1}{\rho}P_D(\boldsymbol{x} - \boldsymbol{x}_p(t), t), \quad \text{for } z = 0, \tag{3.3}$$

$$\eta_t = \phi_z + 2\nu^*\nabla_\perp^2\eta, \quad \text{for } z = 0, \tag{3.4}$$

where ϕ and η denote the velocity potential and the free-surface displacement, respectively. $g(t) = g_0(1 + \gamma/g_0 \cos \omega t)$ is the gravitational acceleration in the bath's frame of reference, P_D denotes the pressure exerted by the drop, $\boldsymbol{x}_p$ denotes the drop's horizontal position, $h(\boldsymbol{x})$ denotes the bottom topography, ν^* is the effective viscosity and $\boldsymbol{n}$ is the unit vector normal to the bottom surface. $\nabla_\perp = (\partial_x, \partial_y)$ denotes the horizontal gradient. The key modification made by Faria (2016) is replacing ϕ_z in (3.4) by $-\nabla_\perp \cdot (\bar{h}\nabla_\perp\phi)$, where $\bar{h}$ is an effective depth chosen to model correctly waves with the Faraday frequency. Over regions of constant depth, $\mathscr{F}[\phi_z(\boldsymbol{x}, 0, t)] = k \tanh(kh)\mathscr{F}[\phi(\boldsymbol{x}, 0, t)]$, where $\mathscr{F}$ denotes the Fourier transform in (x, y). Consequently, in order for the approximation of Faria (2016) to correctly model the wavenumber k_F over a depth h, the effective depth $\bar{h}$ must be

$$\bar{h} = \frac{\tanh k_F h}{k_F}. \tag{3.5}$$

In the reflection experiments, we have

$$h = \begin{cases} h_0 & \text{for } x < 0, \\ h_1 & \text{for } x > 0. \end{cases} \tag{3.6}$$

The effective depth is then given by

$$\bar{h} = \begin{cases} \tanh(k_{F_0}h_0)/k_{F_0} & \text{for } x < 0, \\ \tanh(k_{F_1}h_1)/k_{F_1} & \text{for } x > 0, \end{cases} \tag{3.7}$$

where k_{F_0} and k_{F_1} denote the Faraday wavenumber in the deep and shallow regions, respectively. The phase speed of surface waves in the two regions of the bath of depth h_0 and h_1 is then recovered.

The horizontal motion of the walker is governed by Molacek & Bush (2013b)

$$m\frac{\mathrm{d}^2\boldsymbol{x}_p}{\mathrm{d}t^2} + \left(c_4\sqrt{\frac{\rho R}{\sigma}}F(t) + 6\pi R\mu_{air}\right)\frac{\mathrm{d}\boldsymbol{x}_p}{\mathrm{d}t} = -F(t)\nabla\eta|_{\boldsymbol{x}=\boldsymbol{x}_p}, \tag{3.8}$$

where $F(t)$ denotes the reaction force exerted on the drop by the fluid, R is the drop radius, m is the drop mass, μ_{air} is the viscosity of air, and c_4 the tangential coefficient of restitution, which was measured and reported in Molacek & Bush (2013b). Assuming a resonant walker in the $(2, 1)^2$ mode (see figure 1c), the drop impacting the surface periodically at $t_i = nT_F$, and that the contact time is short relative to the Faraday period, it can be shown (Faria 2016) that the reaction force

is $F(t) = mg \sum_{n=0}^{\infty} \delta(t/T_F + n)$. Finally, the penetration depth of the drop (Milewski *et al.* 2015) is assumed to be infinitesimally small relative to the Faraday wavelength, so that we may write

$$P_D = \frac{F(t)}{\lambda_F^2} \delta\left(\frac{x - x_p}{\lambda_F}\right). \tag{3.9}$$

The final model is then given by

$$\phi_t = -g(t)\eta + \frac{\sigma}{\rho}\nabla_\perp^2 \eta + 2\nu^* \nabla_\perp^2 \phi - \frac{1}{\rho} P_D(x - x_p(t), t), \tag{3.10}$$

$$\eta_t = -\nabla_\perp \cdot (\bar{h}\nabla_\perp \phi) + 2\nu^* \nabla_\perp^2 \eta, \tag{3.11}$$

with P_D given by (3.9), the local depth computed from (3.5), and the drop motion governed by (3.8).

We perform numerical simulations with the parameters used in our experiments. As we do not model the vertical dynamics, the phase of impact φ is determined by requiring that the drop speed in free space correspond to that observed in experiments (Oza, Rosales & Bush 2013). We choose the coefficient of restitution $c_4 = 0.17$, as suggested by Molacek & Bush (2013*a*) for silicone oil of viscosity 20 cSt and forcing frequency 80 Hz. Finally, following Milewski *et al.* (2015) and Blanchette (2016) we use an effective viscosity $\nu^* = 0.8025\nu$ in order to match the value of the Faraday threshold γ_F observed in experiments.

As in our experiments, the simulated walker–boundary interaction has three stages, as depicted in figure 6(*d–f*). Far from the wall, the walker moves as if in free space. As it approaches the wall, the droplet is attracted by the wall and its trajectory deviated accordingly. The perturbed wave field then diverts its path, causing it to turn around. The drop is then attracted to the wall again as it moves away from it, but eventually converges to a constant angle Θ_r. The simulated wave field is compared in figure 6 to the experimental wave field obtained by surface reconstruction (Damiano *et al.* 2016).

Quantitative comparison between the experimental and theoretical 'reflection laws' shows excellent agreement for $\gamma/\gamma_F = 0.900$ (figure 3*c*). In the simulations, we varied the incoming angle from 4° to 80°. The theoretically predicted reflection is also non-specular with $\Theta_r \in [61°, 84°]$ and the observed dependence of Θ_r on Θ_i is successfully recovered. The upward shift in Θ_r for $\gamma/\gamma_F = 0.850$ is also recovered, but the predicted Θ_r is slightly larger than that observed. This small difference might presumably be attributed to uncertainties in the drop diameter and bouncing phase, that are used as inputs for the numerical simulations.

Comparing observed and simulated trajectories for the fast drop ($D = 0.78$ mm) shows a good qualitative agreement at different memories (figure 4*a*). In particular, the reflected trajectories are well captured and tend to the same final angle of reflection Θ_r. The main difference between the two is in the incident phase, where the attraction of the drop to the barrier is less pronounced in the simulations. For the smaller drop with $D = 0.75$ mm, the comparison of trajectories also shows a good agreement at low memory (figure 5*a*). However, differences arise at high memory, where the theoretical model fails to capture the observed complex trajectories, including the loop that leads to reversed reflection (figure 5*b*). The observed looping and reversed reflection only arise in the simulations for an even smaller drop or smaller angle of incidence. This difference may be due to the model assumption of constant bouncing phase, which is known to break down for small drops at high memory (see figure 1*c*) and is also questionable in the vicinity of the barrier.

4. Discussion and conclusion

The reflection of walking droplets from a planar barrier is non-specular: the reflection angle Θ_r differs from the incidence angle Θ_i and is typically in the range $60° < \Theta_r < 80°$. The reflection behaviour is weakly dependent on system parameters such as the forcing amplitude γ/γ_F, the liquid depth h_1 above the barrier, the drop diameter D and speed v. The non-specular reflection has been faithfully captured by a reduced theoretical model that treats the boundaries as zones of reduced wave speed. Despite the relative simplicity of the model, its predictions are in good agreement with the experimental results. Trajectories are reliably reproduced except at extremely high memory, where reversed reflection events arise in the model only for relatively small drops and low Θ_i. This difference may well result from shifts in bouncing phase experienced by the walkers close to the barrier, that are not taken into account by the model.

Non-specular reflection indicates that the walker momentum in the $\hat{y}$-direction, parallel to the wall, is not conserved. In our system, figure 3(*c*) indicates that this *y*-momentum component is always increased by the walker–wall interaction. This increase may be rationalized in terms of the reduced models of walker dynamics developed by Bush *et al.* (2014) and Labousse & Perrard (2014), both of which demonstrate that the walker behaves like a Rayleigh oscillator. Specifically, the wave force acts to restore the walker to its free walking speed, v_0, acting as a drag if the drop speed $v > v_0$, and a propulsive force if $v < v_0$. The trajectory equation developed by Bush *et al.* (2014) takes the form

$$\frac{\mathrm{d}}{\mathrm{d}t}\boldsymbol{p} = D(v)\boldsymbol{v} + \boldsymbol{F}, \tag{4.1}$$

where $\boldsymbol{p} = \gamma_B m \boldsymbol{v}$ is the walker momentum, $\gamma_B(v)$ is the hydrodynamic boost factor associated with the effective added mass of the walker's wave field, $\boldsymbol{F}$ is an external applied force and $D(v)$ is the speed-dependent restoring wave force factor with the key feature that $D(v) > 0$ if $v < v_0$ and $D(v) < 0$ if $v > v_0$. Assuming that the barrier imparts a force only in the perpendicular $\hat{x}$ direction, the change in walker's *y*-momentum over the course of the reflection $\Delta p_y = \int_{-\infty}^{\infty} D(v)v_y\,\mathrm{d}t$. As is evident in figure 6(*g*), the walker–wall interaction acts to slow the drop virtually everywhere; consequently, $D(v) > 0$ along the bulk of the trajectory, and Δp_y is positive definite. The walker is thus seen to acquire *y*-momentum by virtue of the wave force propelling it forward along its slowed path. This perspective will be broadened and made quantitative in an upcoming characterization of an effective 'Snell's law' for walkers experiencing an arbitrary step change in fluid depth.

References

ANDERSEN, A., MADSEN, J., REICHELT, C., AHL, S. R., LAUTRUP, B., ELLEGAARD, C., LEVINSEN, M. T. & BOHR, T. 2015 Double-slit experiment with single wave-driven particles and its relation to quantum mechanics. *Phys. Rev.* E **92** (1), 013006.

BATELAAN, H., JONES, E., HUANG, W. C.-W. & BACH, R. 2016 Momentum exchange in the electron double-slit experiment. *J. Phys. Conf. Series* **701**, 012007.

BLANCHETTE, F. 2016 Modeling the vertical motion of drops bouncing on a bounded fluid reservoir. *Phys. Fluids* **28** (3), 032104.

BUSH, J. W. M. 2015a The new wave of pilot-wave theory. *Phys. Today* **68**, 47–53.

BUSH, J. W. M. 2015b Pilot-wave hydrodynamics. *Annu. Rev. Fluid Mech.* **49**, 269–292.

BUSH, J. W. M., OZA, A. U. & MOLÁCEK, J. 2014 The wave-induced added mass of walking droplets. *J. Fluid Mech.* **755**, R7.

COUDER, Y. & FORT, E. 2006 Single particle diffraction and interference at a macroscopic scale. *Phys. Rev. Lett.* **97**, 154101.

COUDER, Y., PROTIÈRE, S., FORT, E. & BOUDAOUD, A. 2005 Dynamical phenomena: walking and orbiting droplets. *Nature* **437**, 208.

DAMIANO, A., BRUN, P.-T., HARRIS, D. M., GALEANO-RIOS, C. & BUSH, J. W. M. 2016 Surface topography measurements of the bouncing droplet experiment. *Exp. Fluids* (submitted).

EDDI, A., FORT, E., MOISY, F. & COUDER, Y. 2009 Unpredictable tunneling of a classical wave-particle association. *Phys. Rev. Lett.* **102**, 240401.

EDDI, A., SULTAN, E., MOUKHTAR, J., FORT, E., ROSSI, M. & COUDER, Y. 2011 Information stored in Faraday waves: the origin of path memory. *J. Fluid Mech.* **674**, 433–463.

FARADAY, M. 1831 On the forms and states of fluids on vibrating elastic surfaces. *Phil. Trans. R. Soc. Lond.* **121**, 319–340.

FARIA, L. 2016 A model for Faraday pilot-waves over variable topography. *J. Fluid Mech.* (submitted).

FORT, E., EDDI, A., BOUDAOUD, A., MOUKHTAR, J. & COUDER, Y. 2010 Path-memory induced quantization of classical orbits. *Proc. Natl Acad. Sci. USA* **107** (41), 17515–17520.

GILET, T. 2014 Dynamics and statistics of wave-particle interactions in a confined geometry. *Phys. Rev.* E **90** (5), 052917.

GILET, T. 2016 Quantumlike statistics of deterministic wave-particle interactions in a circular cavity. *Phys. Rev.* E **93** (4), 042202.

HARRIS, D. 2015, The pilot-wave dynamics of walking droplets in confinement. PhD thesis, Massachusetts Institute of Technology.

HARRIS, D. & BUSH, J. W. M. 2014 Droplets walking in a rotating frame: from quantized orbits to multimodal statistics. *J. Fluid Mech.* **739**, 444–464.

HARRIS, D. & BUSH, J. W. M. 2015 Generating uniaxial vibration with an electrodynamic shaker and external air bearing. *J. Sound Vib.* **334**, 255–269.

HARRIS, D., LIU, T. & BUSH, J. W. M. 2015 A low-cost, precise piezoelectric droplet-on-demand generator. *Exp. Fluids* **56**, 83–90.

HARRIS, D., MOUKHTAR, J., FORT, E., COUDER, Y. & BUSH, J. W. M. 2013 Wavelike statistics from pilot-wave dynamics in a circular corral. *Phys. Rev.* E **88**, 011001(R).

LABOUSSE, M. 2014 Etude d'une dynamique à mémoire de chemin: une expérimentation thórique. PhD thesis, Université Paris 6.

LABOUSSE, M., OZA, A. U., PERRARD, S. & BUSH, J. W. M. 2016 Pilot-wave dynamics in a harmonic potential: quantization and stability of circular orbits. *Phys. Rev.* E **93** (3), 033122.

LABOUSSE, M. & PERRARD, S. 2014 Non-Hamiltonian features of a classical pilot-wave dynamics. *Phys. Rev.* E **90** (2), 022913.

LABOUSSE, M., PERRARD, S., COUDER, Y. & FORT, E. 2014 Build-up of macroscopic eigenstates in a memory-based constrained system. *New J. Phys.* **16** (11), 113027.

MILEWSKI, P., GALEANO-RIOS, C., NACHBIN, A. & BUSH, J. W. M. 2015 Faraday pilot-wave hydrodynamics: modeling and computation. *J. Fluid Mech.* **778**, 361–388.

MOLACEK, J. & BUSH, J. W. M. 2013a Droplets bouncing on a vibrating fluid bath. *J. Fluid Mech.* **727**, 582–611.

MOLACEK, J. & BUSH, J. W. M. 2013b Droplets walking on a vibrating fluid bath: towards a hydrodynamic pilot-wave theory. *J. Fluid Mech.* **727**, 612–647.

OZA, A., HARRIS, D. M., ROSALES, R. R. & BUSH, J. W. M. 2014 Pilot-wave dynamics in a rotating frame: on the emergence of orbital quantization. *J. Fluid Mech.* **744**, 404–429.

OZA, A., ROSALES, R. R. & BUSH, J. W. M. 2013 A trajectory equation for walking droplets: a hydrodynamic pilot-wave theory. *J. Fluid Mech.* **737**, 552–570.

PERRARD, S., LABOUSSE, M., FORT, E. & COUDER, Y. 2014*a* Chaos driven by interfering memory. *Phys. Rev. Lett.* **113**, 104101.

PERRARD, S., LABOUSSE, M., MISKIN, M., FORT, E. & COUDER, Y. 2014*b* Self-organization into quantized eigenstates of a classical wave-driven particle. *Nature Comm.* **5**, 3219.

PROTIÈRE, S., BOUDAOUD, A. & COUDER, Y. 2006 Particle wave association on a fluid interface. *J. Fluid Mech.* **554**, 85–108.

WIND-WILLASSEN, O., MOLACEK, J., HARRIS, D. M. & BUSH, J. W. M. 2013 Exotic states of bouncing and walking droplets. *Phys. Fluids* **25**, 082002.